Journal and Proceedings of the Royal Society of New South Wales, vol. 145, nos. 443 & 444, pp. 66-74.
ISSN 0035-9173/12/010066-9

Realisation of a single-atom transistor in silicon

Martin Fuechsle[1*], Jill A. Miwa[1], Suddhasatta Mahapatra[1], Oliver Warschkow[2], Lloyd C. L. Hollenberg[3], Michelle Y. Simmons[1]

[1] Centre for Quantum Computation and Communication Technology, University of New South Wales, Sydney, NSW 2052, Australia
[2] Centre for Quantum Computation and Communication Technology, University of Sydney, Sydney, NSW 2006, Australia
[3] Centre for Quantum Computation and Communication Technology, University of Melbourne, VIC 3010, Australia

* Corresponding author.
E-mail: martin.fuechsle@unsw.edu.au

***Editor's note**: Martin Fuechsle won one of the Royal Society of New South Wales' Scholarships in 2011. This paper describes the work that was recognised in the Award.*

Abstract

We demonstrate the fabrication of a single-atom transistor based on an individual phosphorus (P) donor atom in a crystalline silicon environment. Using a scanning tunnelling microscopy (STM)-based lithography approach, the single atom is deterministically placed with a spatial accuracy of one silicon lattice site within a gated transport device. Electronic measurements at liquid Helium temperatures and below confirm the presence of the single P donor and show that the donor's charge state can be precisely controlled via gate voltages. We observe a charging energy that is remarkably similar to the value expected for isolated P donors in bulk silicon, which is in sharp contrast to previous experiments on single-dopant transport devices. The unprecedented accuracy and high level of control over the electrostatic device properties afforded by our fabrication method opens the door for a scalable donor-based quantum processing architecture in silicon.

Keywords: silicon, quantum computation, scanning tunnelling microscopy (STM), STM lithography, single-atom devices

Introduction

Down-scaling has been the leading paradigm of the semiconductor industry ever since the invention of the first transistor in 1947 (Moore 1965). Miniaturisation of the single most important building block of modern silicon-based electronic devices – the field-effect transistor (FET) – has advanced to a stage where characteristic dimensions are approaching the 10nm-scale. In this regime, device performance can depend on the number and the discrete distribution of individual dopants (Roy 2005), i.e. foreign atoms that are added to semiconductors in small quantities to alter the electronic properties of the host material. Consequently, being able to control dopant density and distribution on a sub-nm level will be crucial for further scaling of conventional integrated nanoelectronic devices.

The realisation that "traditional" miniaturisation of conventional silicon devices by geometric scaling will soon reach its ultimate limit (set by the discreteness of matter) has lead to intensified research in alternative approaches to enhance the computational power of logic devices. One of the most exciting of these emerging technologies is quantum computation – a novel concept of computation where information is stored in coherent superpositions of suitable quantum mechanical states, so-called quantum bits or qubits. An essential requirement for the realisation of a physical qubit is the need to preserve the coherence between these basis states long enough to be able to perform logic operations (DiVincenzo (1998)).

The spin states associated with donors (i.e. dopants that donate their valence electron to the host material) in silicon are a promising candidate for the realisation of quantum logic devices due to their resilience against decoherence (Feher (1959), Tyryshkin et al. 2003)). This is essentially due to two desirable material properties of silicon (Kane (1998)), the predominance of spin-zero ^{28}Si nuclei and a small spin-orbit coupling. As a result, various silicon-based quantum computer architectures have been proposed, using either the nuclear spin (Kane (1998)), or donor electron spin (Vrijen et al. (2000)) or charge (Hollenberg et al. 2004) of individual phosphorus dopants to define the qubit. However, while considerable progress has recently been made towards spin manipulation and spin read-out (Morello et al. 2010), a remaining challenge is the scale-up of donor-based devices towards a 'useful' quantum computer comprising a large number of qubits (DiVincenzo 1998). While proposals exist for scalable two-dimensional architectures (Hollenberg et al. (2006)), these rely on vast arrays of individual impurities. To avoid spatial oscillations in the exchange coupling between neighbouring donor sites arising from the silicon bandstructure (Koiller et al. (2002)), these architectures require precise control over the location of each dopant atom within the array. A key challenge in fabricating a functional donor-based qubit is therefore the ability to pattern individual impurities in an epitaxial silicon environment with atomic accuracy.

Here, we demonstrate how STM hydrogen lithography can be used as a viable tool to overcome this challenge since it allows individual dopants to be patterned within a functional transport structure with a spatial accuracy of one lattice site.

Sample fabrication

The tool that is central to our fabrication method is a scanning tunnelling microscope (Binnig and Rohrer (1982)). Here, a fine metallic tip is scanned over a conducting surface in a raster motion in an ultra-high vacuum (UHV) environment. By plotting the measured tunnelling current between the tip and the substrate as a function of the position, it is possible to generate a map of the surface with sub-nanometre resolution. To fabricate functional devices, we use a lithographic approach based on the STM's ability to remove hydrogen (H) atoms from a silicon (Si) surface with atomic precision (Lyding et al. (1994)).

One of the key advantages of using STM for device fabrication is that it can be turned from a surface patterning tool into a non-invasive imaging tool simply by adjusting the voltage applied to the tip. This allows us to image the structure at every step of the patterning process. Fig. 1a illustrates the fabrication of the dopant-based transport structure. Here, the 3D perspective representation shows an STM image of the

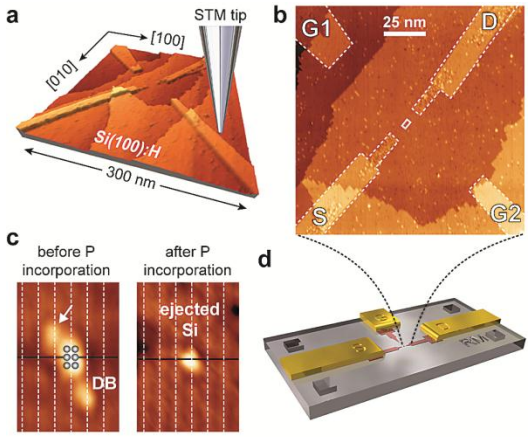

Figure 2: Incorporation pathway for a single P atom. Schematic illustration of the reaction pathway from a phosphine molecule (PH_3) to the incorporated single phosphorus atom. Upon adsorption at room temperature, PH_3 immediately dissociates to PH_2 + H (left panel) and eventually loses its remaining H atoms to neighbouring Si sites as pictured. A quick anneal at 350 °C prompts the remaining P atom to substitute for a silicon atom in the surface layer underneath, ejecting a silicon adatom in the process. It is this ejected Si atom that is observed in the STM images after the incorporation reaction (right panel of Fig. 1c). We find that 3 adjacent dimers (i.e. 6 bare Si sites) along one dimer row are necessary to incorporate exactly one phosphorus atom.

hydrogen terminated Si surface (cleaved along the (100) crystal direction) where the STM tip has been used to selectively desorb a four-terminal structure. In a subsequent step, these regions will be dosed with phosphine gas (PH_3) to form phosphorus-doped co-planar transport electrodes where the dopants are essentially confined to a single atomic plane in the perpendicular (z-) direction. Due to the high doping density (where 1 out of 4 Si atoms within the plane is replaced by a P dopant), the STM-patterned regions will conduct down to cryogenic temperatures while the surrounding substrate becomes insulating due to the thermal freeze-out of mobile carriers. This fabrication method has previously enabled the fabrication of dopant-based quantum dot structures, i.e. isolated doped islands containing a number of donors ranging from several 1000 (Fuhrer et al. (2009)) down to a few (Fuechsle et al. (2010).

Fig. 1b is a close-up of the inner device region showing the source (S) and drain (D) leads for electric measurements. These are precisely aligned to a single phosphorus donor that has been incorporated in the centre of the device (indicated by the white rectangle). Two in-plane gates (G1 and G2) are patterned on either side of the S-D transport channel to control the electrostatic potential at the position of the donor. These control gates are patterned further away (at a distance of 54 nm from the donor site) to avoid gate leakage currents from direct tunnelling to the leads.

The incorporation pathway from the adsorbed phosphine molecules on the bare Si surface to the incorporated P donors is well-understood (Wilson et al. (2004), Warschkow et al. (2005)) and occurs as a sequence of dissociative processes as illustrated in Fig. 2.

$$PH_3(ads) \rightarrow PH_2+H \rightarrow PH+2H \rightarrow P+3H \rightarrow P(incorp)$$

Here, the chemisorbed PH_3 successively loses all 3 H atoms to neighbouring bare Si sites. Upon thermal activation (by briefly annealing the substrate at 350 °C), the remaining P atom on the silicon surface incorporates into the Si surface, ejecting a silicon adatom in the process. Importantly, we find that 3 adjacent dimers (i.e. pairs of Si surface atoms) along one dimer row are necessary to incorporate precisely one P atom, in agreement with theoretical predictions (Wilson et al. (2004)) as well as previous incorporation experiments (Schofield et al. (2003)). We should note that due to the limited number of bare Si sites, only one P atom can incorporate within the

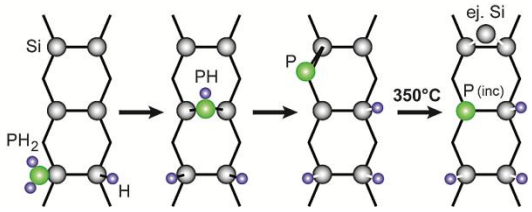

Figure 2: Incorporation pathway for a single P atom. Schematic illustration of the reaction pathway from a phosphine molecule (PH_3) to the incorporated single phosphorus atom. Upon adsorption at room temperature, PH_3 immediately dissociates to PH_2 + H (left panel) and eventually loses its remaining H atoms to neighbouring Si sites as pictured. A quick anneal at 350 °C prompts the remaining P atom to substitute for a silicon atom in the surface layer underneath, ejecting a silicon adatom in the process. It is this ejected Si atom that is observed in the STM images after the incorporation reaction (right panel of Fig. 1c). We find that 3 adjacent dimers (i.e. 6 bare Si sites) along one dimer row are necessary to incorporate exactly one phosphorus atom.

3-dimer patch, even if the surface is saturation dosed so that initially 3 PH_2 are adsorbed within the patch (see Fuechsle et al. (2012). A high-resolution image of the designated single donor incorporation site in the centre of our device is shown in Fig. 1c, both before (left panel) and after (right panel) the dosing and incorporation anneal cycle. In the left panel, we can clearly identify the required 6 H-desorbed bare Si sites. Upon dosing with PH_3 and a ~5 s incorporation anneal at 350°C, we observe a clear change in the surface morphology (right panel). Here, the successful incorporation of a single P donor is evidenced by the observation of a single Si adatom which appears as a bright protrusion centred on a dimer row (Brocks et al. (1992)). Since the incorporated P atom substitutes for one of the 6 Si atoms within the 3-dimer site, the lateral spatial patterning accuracy of our method corresponds to ±1 Si lattice site (±3.8 Å).

The fabrication of the single-atom transistor is achieved in a two-step process: First, the intended incorporation area for the central single donor is desorbed along with the innermost parts of the leads. After an initial phosphine dosing and incorporation anneal cycle, the area is imaged again to verify the successful incorporation of a single P. Next, the in-plane gates are aligned and desorbed along with the extensions of the leads as shown in Fig. 1b. After a second dosing and incorporation anneal cycle, the entire device is overgrown with ~180 nm silicon to activate the dopants and to remove the structure away from detrimental surface effects. The low sample temperature during overgrowth (250 °C) maintains the structural integrity of the Si:P structure and minimises dopant segregation (Oberbeck et al. (2004)). The sample is then removed from the UHV system and *ex-situ* metallic leads are defined over the STM-patterned dopant regions to form ohmic contacts to the buried dopant structure underneath, as illustrated in Fig. 1d.

Device characterisation

The transport properties of our single donor device were characterised in a $^3He/^4He$ dilution refrigerator at milliKelvin temperatures. In this temperature regime, the frozen-out intervening silicon substrate constitutes a tunnel barrier between the electrodes such that electronic transport from S to D occurs via the discrete quantum states of the donor between the leads. The inset of Fig. 3 shows the measured gate leakage current for both gates (flowing from each gate to any of the other electrodes) as a function of the applied gate voltage. We find that the available gate range is smaller for the narrower gate, G2. This is possibly due to a higher potential gradient around the tip of a narrow electrode which results in a smaller

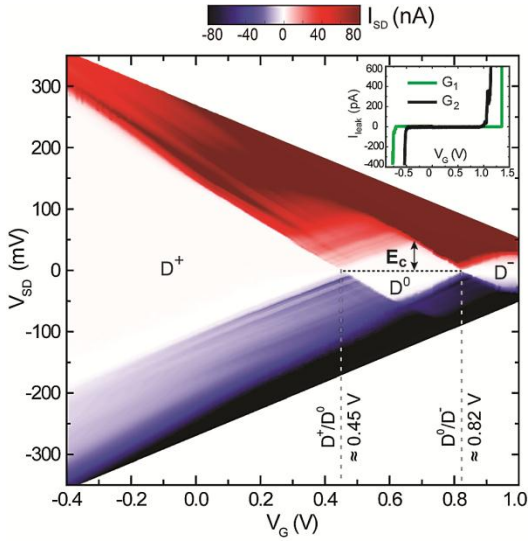

Figure 3: Stability diagram of a single-atom transistor.
The graph shows the measured source-drain current I_{SD} plotted as a function of bias voltage V_{SD} and gate voltage V_G (applied to both gates in parallel). The measurement was performed at a sample temperature of ~50 milliKelvin. In the diamond-shaped regions (centred around the V_{SD} = 0 axis), conduction through the device is suppressed due to Coulomb blockade, and the number of electrons bound to the central P atom is fixed. By applying a voltage to the gate electrodes, it is thus possible to switch the current from zero (central white regions) to a finite value (blue, red regions). We can clearly identify the three possible charge states of the donor, the ionised D^+ state, the charge-neutral D^0 state (with one bound electron), and the negatively charged D^- state, where two electrons are bound to the donor. The height of the D^0 diamond yields the charging energy E_C = 47 ± 3 meV, which is required to add the second electron to the donor. To limit the maximum current through the device, the bias voltage window was decreased as V_G was made more positive, resulting in a trapezoidal plot. Inset: The leakage current I_{leak} as a function of the applied gate voltage. The effective gate range for each gate is determined by the region where I_{leak} is negligible.

effective tunnel barrier. The leakage curves for both gates are asymmetric for positive and negative gate voltages with a significantly higher breakthrough voltage for $V_G > 0$. This is consistent with findings from previous donor-based quantum dot devices (Fuhrer et al. (2009)) and may result from partial depletion of the gate electrodes for large positive voltages.

In Fig. 3, the dc source-drain current I_{SD} is plotted as a function of the bias voltage V_{SD} and gate voltage V_G (applied to gates G1 and G2 in parallel). In this so-called stability diagram, the conductance of the single-atom transistor is zero in the diamond-shaped (white) regions due to Coulomb blockade. The latter refers to the suppression of current when the energy required to add an extra electron to a conducting island (the so-called charging energy) exceeds the thermal energy of the electrons in the leads. In our case, the island is defined by the single donor in the centre of the device. We find that the "diamond" for $V_G < 450$ mV does not close, i.e. the blockaded bias region increases nearly linearly with decreasing gate voltage all the way down to the lower end of the gate range. This is the expected behaviour for the positively ionised state (commonly referred to as the D^+ state) of a single P donor which cannot lose more that its one valence electron (Lansbergen et al. 2008). We thus identify the two other charge-stable regions in Fig. 3 as the charge-neutral D^0 state (for 450 mV < V_G < 820 mV) and the two-electron D^- state (V_G > 820 mV) of the donor, respectively. The current flowing from source to drain can thus be modulated by applying a voltage to the control gates, so that the device indeed behaves like a transistor.

For our single-donor device, we can directly extract the charging energy, E_C, from the transport data of Fig. 3. The charging energy is given by the height of the D^0 Coulomb diamond (Kouwenhoven et al. 1996), for which we find 47 ± 3 meV. The error arises from the asymmetry of the diamond height

for $V_{SD} > 0$ and $V_{SD} < 0$ which we attribute to a different capacitive coupling of the one- and two-electron donor states to the electrodes. Importantly, the experimental value for E_C in our device is remarkably similar to the value expected for isolated P donors based on the binding energies determined by optical absorption spectroscopy (45.6 meV for D^0 and ~1.7 meV for D^-, respectively) in bulk Si (Ramdas and Rodriguez (1981)). This is in sharp contrast to previous single-dopant transport devices in silicon which have revealed charging energies that significantly differ from the bulk case (Lansbergen et al. 2008, Pierre et al. 2010, Rahman et al. (2011)). In these previous experiments, the difference was attributed either to screening effects resulting from strong capacitive coupling to a nearby gate (Lansbergen et al. 2008) or strong electric fields (Rahman et al. 2011), or to an enhanced donor ionisation energy in the proximity of a dielectric interface (Pierre et al. (2010)). However, both effects are expected to be small for our phosphorus dopant which is symmetrically positioned between the two gates (resulting in a negligible gate electric field) and encapsulated deep within a crystalline silicon environment.

The transitions between the different charge states of the donor in Fig. 3 reproducibly occur at the same gate voltages, ≈ 0.45 mV for the $D^+ \leftrightarrow D^0$ transition and ≈ 0.82 mV for the $D^0 \leftrightarrow D^-$ transition, respectively. The particular positions of the transition points along the gate axis reflect the inherent influence of the highly-doped leads in our transport device. We have quantified this influence by calculating the quantum states of the central P donor as a function of the (gate voltage-dependent) electrostatic potential defined by the electrodes (for details see Fuechsle et al. 2012). Indeed, we find that the calculated transition gate voltages are in excellent agreement with the experimental values. Furthermore, the calculations fully support the bulk-like charging energy measured in our single-donor device. The remarkable agreement between our multi-scale modelling approach and the experimental observations is testament to the high level of control over the electrostatic device properties afforded by our atomically precise fabrication method.

Conclusions

We have demonstrated the fabrication of a single-donor device in silicon, where an individual phosphorus atom is deterministically placed with sub-nm scale accuracy between dopant-based transport electrodes. Electronic measurements at cryogenic temperatures reveal that transport in our device occurs through the discrete states of the central P donor and that we can precisely control the donor's charge state via a voltage applied to the control gates. In particular, for our single-donor device we find a charging energy that is remarkably similar to the value expected for isolated donors in a bulk silicon environment. We attribute this to the absence of nearby metallic gates or interfaces and the vanishing gate electric field afforded by our device design.

With miniaturisation of classical silicon nanoelectronic devices steadily approaching the 10nm-regime, controlling the doping profile as well as the location of individual dopants will be crucial for continued developments in both quantum and classical devices in silicon. The fabrication technique presented here opens the door for novel device concepts which use single dopant atoms as their active elements. In particular, our work presents an important step towards the realisation of a scalable donor-based qubit architecture.

Acknowledgements

We would like to thank S. Rogge, J. Verduijn, and J. Mol for useful discussions. Martin Fuechsle has been supported in part by an Endeavour International Postgraduate Research Scholarship. This research was conducted by the Australian Research Council Centre of Excellence for Quantum Computation and Communication Technology (project no. CE110001027). The research was supported by the US Army Research Office (contract no. W911NF08-1-0527). M. Y. Simmons acknowledges a Federation Fellowship.

References

Binnig, G. & Rohrer, H. (1982) Scanning Tunneling Microscopy; *Helvetica Physica Acta*; **55**, 6, 726-735.

Brocks, G., Kelly, P. J. & Car, R. (1992) The energetics of adatoms on the Si(100) surface; *Surface Science*; **269**, 860-866.

DiVincenzo, D. P. (1998) Real and realistic quantum computers; *Nature*; **393**, 6681, 113-114.

Feher, G. (1959) Electron spin resonance experiments on donors in silicon. 1. Electronic structure of donors by the electron nuclear double resonance technique; *Physical Review*; **114**, 5, 1219-1244.

Fuechsle, M., Mahapatra, S., Zwanenburg, F. A., Friesen, M., Eriksson, M. A. & Simmons, M. Y. (2010) Spectroscopy of few-electron single-crystal silicon quantum dots; *Nature Nanotechnology*; **5**, 7, 502-505.

Fuechsle, M., Miwa, J. A., Mahapatra, S., Ryu, H., Lee, S., Warschkow, O., Hollenberg, L. C. L., Klimeck, G. & Simmons, M. Y. (2012) A single-atom transistor; *Nature Nanotechnology*; **7**, 242–246.

Fuhrer, A., Fuchsle, M., Reusch, T. C. G., Weber, B. & Simmons, M. Y. (2009) Atomic-scale, all epitaxial in-plane gated donor quantum dot in silicon; *Nano Letters*; **9**, 2, 707-710.

Hollenberg, L. C. L., Dzurak, A. S., Wellard, C., Hamilton, A. R., Reilly, D. J., Milburn, G. J. & Clark, R. G. (2004) Charge-based quantum computing using single donors in semiconductors; *Physical Review B*; **69**, 11, 4.

Hollenberg, L. C. L., Greentree, A. D., Fowler, A. G. & Wellard, C. J. (2006) Two-dimensional architectures for donor-based quantum computing; *Physical Review B*; **74**, 4, 045311.

Kane, B. E. (1998) A silicon-based nuclear spin quantum computer; *Nature*; **393**, 6681, 133-137.

Koiller, B., Hu, X. D. & Das Sarma, S. (2002) Exchange in silicon-based quantum computer architecture; *Physical Review Letters*; **88**, 2, 027903.

Kouwenhoven, L. P., Marcus, C. M., McEuen, P. L., Tarucha, S., Westervelt, R. M. & Wingreen, N. S. (1996) *Electron transport in quantum dots*, 105-214.

Lansbergen, G. P., Rahman, R., Wellard, C. J., Woo, I., Caro, J., Collaert, N., Biesemans, S., Klimeck, G., Hollenberg, L. C. L. & Rogge, S. (2008) Gate-induced quantum-confinement transition of a single dopant atom in a silicon FinFET; *Nature Physics*; **4**, 8, 656-661.

Lyding, J. W., Shen, T. C., Hubacek, J. S., Tucker, J. R. & Abeln, G. C. (1994) Nanoscale patterning and oxidation of H-passivated Si(100)-2x1 surfaces with an ultrahigh-vacuum scanning tunneling microscope; *Applied Physics Letters*; **64**, 15, 2010-2012.

Moore, G. E. (1965) Cramming more components onto integrated circuits; *Electronics*; **38**, 114-117.

Morello, A., Pla, J. J., Zwanenburg, F. A., Chan, K. W., Tan, K. Y., Huebl, H., Mottonen, M., Nugroho, C. D., Yang, C. Y., van Donkelaar, J. A., Alves, A. D. C., Jamieson, D. N., Escott, C. C., Hollenberg, L. C. L., Clark, R. G. & Dzurak, A. S. (2010) Single-shot readout of an electron spin in silicon; *Nature*; **467**, 7316, 687-691.

Oberbeck, L., Curson, N. J., Hallam, T., Simmons, M. Y., Bilger, G. & Clark, R. G. (2004) Measurement of phosphorus segregation in silicon at the atomic scale using scanning tunneling microscopy; *Applied Physics Letters*; **85**, 8, 1359-1361.

Pierre, M., Wacquez, R., Jehl, X., Sanquer, M., Vinet, M. & Cueto, O. (2010) Single-donor ionization energies in a nanoscale CMOS channel; *Nature Nanotechnology*; **5**, 2, 133-137.

Rahman, R., Lansbergen, G. P., Verduijn, J., Tettamanzi, G. C., Park, S. H., Collaert, N., Biesemans, S., Klimeck, G., Hollenberg, L. C. L.

& Rogge, S. (2011) Electric field reduced charging energies and two-electron bound excited states of single donors in silicon; *Physical Review B*; **84**, 11, 115428.

Ramdas, A. K. & Rodriguez, S. (1981) Spectroscopy of the solid-state analogs of the hydrogen atom: donors and acceptors in semiconductors; *Reports on Progress in Physics*; **44**, 12, 1297-1387.

Roy, S. & Asenov, A. (2005) Where do the dopants go?; *Science*; **309**, 5733, 388-390.

Schofield, S. R., Curson, N. J., Simmons, M. Y., Ruess, F. J., Hallam, T., Oberbeck, L. & Clark, R. G. (2003) Atomically precise placement of single dopants in Si; *Physical Review Letters*; **91**, 13, 136104.

Tan, K. Y., Chan, K. W., Mottonen, M., Morello, A., Yang, C. Y., van Donkelaar, J., Alves, A., Pirkkalainen, J. M., Jamieson, D. N., Clark, R. G. & Dzurak, A. S. (2010) Transport Spectroscopy of Single Phosphorus Donors in a Silicon Nanoscale Transistor; *Nano Letters*; **10**, 1, 11-15.

Tyryshkin, A. M., Lyon, S. A., Astashkin, A. V. & Raitsimring, A. M. (2003) Electron spin relaxation times of phosphorus donors in silicon; *Physical Review B*; **68**, 19, 193207.

Vrijen, R., Yablonovitch, E., Wang, K., Jiang, H. W., Balandin, A., Roychowdhury, V., Mor, T. & DiVincenzo, D. (2000) Electron-spin-resonance transistors for quantum computing in silicon-germanium heterostructures; *Physical Review A*; **62**, 1, 012306.

Warschkow, O., Wilson, H. F., Marks, N. A., Schofield, S. R., Curson, N. J., Smith, P. V., Radny, M. W., McKenzie, D. R. & Simmons, M. Y. (2005) Phosphine adsorption and dissociation on the Si(001) surface: An ab initio survey of structures; *Physical Review B*; **72**, 12, 125328.

Wilson, H. F., Warschkow, O., Marks, N. A., Schofield, S. R., Curson, N. J., Smith, P. V., Radny, M. W., McKenzie, D. R. & Simmons, M. Y. (2004) Phosphine dissociation on the Si(001) surface; *Physical Review Letters*; **93**, 22, 226102.

Martin Fuechsle
Jill A. Miwa
Suddhasatta Mahapatra
Oliver Warschkow
Lloyd C. L. Hollenberg
Michelle Y. Simmons

(Manuscript received 16 April 2012; accepted 7 July 2012.)

Dr Martin Fuechsle is a Research Fellow at the Centre for Quantum Computation and Communication Technology.

Dr Jill Miwa is a Research Fellow at the Centre for Quantum Computation and Communication Technology.

Dr Suddhasatta Mahapatra is a Senior Research Fellow at the Centre for Quantum Computation and Communication Technology.

Dr Oliver Warschkow is a Senior Research Fellow at the Centre for Quantum Computation and Communication Technology.

Professor Lloyd Hollenberg is Deputy Director at the Centre for Quantum Computation and Communication Technology. He is a Professor of Physics at the University of Melbourne and is an Australian Professorial Fellow.

Professor Michelle Simmons is Director of the Centre for Quantum Computation and Communication Technology. She is the Scientia Professor of Physics at the University of New South Wales and is a Federation Fellow.